

Cobalt Chromium Vanadium Layered Triple Hydroxides as Efficient Oxygen Electrocatalyst for Alkaline Seawater Splitting

Sakila Khatun^{a,b} and Poulomi Roy^{a,b*}

^aMaterials Processing & Microsystems Laboratory, CSIR – Central Mechanical Engineering Research Institute (CMERI), Mahatma Gandhi Avenue, Durgapur 713209, West Bengal, India.

^bAcademy of Scientific and Innovative Research (AcSIR), Ghaziabad, Uttar Pradesh- 201 002, India.

*Email: poulomiroy@yahoo.com, p.roy@cmeri.res.in

Experimental Section

Material synthesis

During experiments all chemicals were used without any purification and aqueous solution was prepared by using ultrapure milli-Q water. At room temperature, 2 mM Cobalt (II) chloride hexahydrate (Merck, $\geq 98\%$) and 1 mM chromium (III) chloride hexahydrate (Merck, $\geq 96\%$) were mixed into 40 ml aqueous solution, followed by addition of 15 mM urea (Merck, $\geq 99.5\%$) into the solution with rigorous mixing until a clear solution was obtained. The as prepared solution was transferred to an autoclave and treated at 120 °C in an oven for 16 h. After completion of reaction, the autoclave was cooled down to room temperature naturally and the black coloured product was collected and washed several times by using milli-Q water and ethanol and lastly the powder sample was dried at naturally.

A series of CoCrV LTHs were prepared in similar way using ammonium vanadium oxide as vanadium (V) source in addition of the Co- and Cr- precursors as described above. The vanadium (V) was added into the solution by varying molar ratios of Cr : V as 4:1, 2:1 and 1:1 keeping Co-precursor concentration same in the aqueous solution. While the bimetallic CoCr-LDH is abbreviated as CC, the LTH series are abbreviated as CCV-1, CCV-

2 and CCV-3 as the detailed reaction parameters and molar concentrations are tabulated in Table S1. To achieve LDH or LTH structures, the reaction duration was optimized in each cases as mentioned in Table S1. After the completion of reactions, the grey coloured samples were collected, washed and dried by similar way as discussed for CoCr-LDH.

Structural characterisation

The composition and phase purity of the obtained samples were recorded by powder X-ray diffraction (Rigaku Miniflex-600) technique using Cu K ∞ source ($\lambda = 1.5418 \text{ \AA}$) within diffraction angle $10^\circ - 80^\circ$. The size and morphology of the as prepared materials were studied by field emission scanning electron microscopy (FE-SEM, Carl Zeiss, Germany) operating at 5 kV. Energy dispersive spectrum (EDX) was characterized to know the elemental composition with atomic% of the materials which associated with FE-SEM apparatus. High resolution transmission electron microscopy (FEI TECNAI 20 G2, Netherlands) characterisation was operated to figure out the micro structural properties of the sample, performing at 200 kV. The TEM specimen was prepared by dispersing little bit powder sample into pure ethanol and a drop of homogeneous solution was deposited on carbon coated Cu grid, certainly drying overnight in vacuum environment. The elemental states of the samples were carried out by XPS measurement on a SCIENTA, R-3000 analyzer with monochromatic Al K α radiation regarding 1.486 KeV energy. The vacuum ambit of the chamber was 1×10^{-10} Torr in the interim of XPS analysis. The binding energy of the sample was calibrated with reference to C1s peak near to 284.6 eV and spectrum were collected considering Co, Cr, V, O and C elements. Fourier transform infrared spectroscopy (FTIR) of the sample was performed by (IR Prestige-21, SHIMADZU) with an ATR spectrum ranges from 400 cm^{-1} to 4000 cm^{-1} . The surface profile of the samples was analyzed using atomic force microscopy (AFM) on Nanosurf 3000 instrument. The AFM specimen was prepared by drop-casting low concentrate homogeneous solution on clean

Si wafer. Raman analysis of the prepared samples was conducted using alpha300 RAS (WITec) Raman spectrometer.

Electrochemical measurements

Electrochemical activities of LTH samples were performed on Biologic SP-150 appearing in standard three electrode system against regular environment. The three electrode configuration consists of a Pt wire and saturated Ag/AgCl as counter and reference electrode, and the developed material on NF was used as working electrode. The electrocatalytic activity of the sample was evaluated in alkaline 1 M KOH, 1M KOH + 1M NaCl, 0.5 M KOH + 0.5 M NaCl and 1 M KOH + seawater electrolyte solutions. The real seawater was collected from the sea shore (*Digha, West Bengal, India*) of Bay of Bengal and the geographical location has been shared in [Figure S10](#). The working electrode was prepared making homogeneous ink of the powder sample (2 mg) mixing in 900 μ l homogeneous solution of isopropanol and water followed by addition of 100 μ l PVDF solutions as binder under ultrasonication and drop casted on bare Ni foam ($2 \times 0.5 \text{ cm}^2$). Prior to drop casting, the NF was treated with 1 M HCl solution to remove the native oxide layer and cleaned by DI water and ethanol. The mass loading of electrocatalysts on the NF was maintained in the range of 1.0-1.2 mg cm^{-2} . The commercial 20 wt% RuO₂ was used with mass loading of 1.1 mg cm^{-2} on NF by identical approach for comparative study.

In electrochemical study, the applied potential corresponding to saturated Ag/AgCl electrode was converted into reversible hydrogen electrode (RHE) by using the given equation:

$$E_{\text{RHE}} = E_{\text{apply}} + E_{\text{Ag/AgCl}} + 0.059 \times \text{pH} \quad (1)$$

The linear sweep voltammetry (LSV) of the catalyst was performed at 1 mV s^{-1} scan rate in a potential range 0 to 0.8 V with respect to standard Ag/AgCl reference electrode in three electrode system. The LSV plots were undergone with 100% iR correction to avoid the

uncompensated series resistance of the electrochemical circuit. The overpotential (η) of water oxidation was calculated by η (V) = 1.23 – E_{RHE} and the intrinsic catalytic parameter Tafel slope (b) was measured from $\eta = a + b \log j$ equation. Electrochemical impedance spectroscopy (EIS) of as prepared sample was conducted around 370 mV overpotential in the frequency range of 10 kHz to 200 mHz. The iR compensated polarisation curves were plotted by using following equation:

$$E_{iR} = E_{RHE} - iR_s \quad (2)$$

Where R_s is equivalent series resistance and can be obtained from EIS fitted plot following a particular electrochemical circuit. Electrochemical active surface area (ECSA) is a valuable parameter to realize definite information on active sites of the catalyst. Cyclic voltammetry (CV) was carried out in non-Faradaic region at different sweep rates from 20 mV s^{-1} to 200 mV s^{-1} to standardize double layer capacitance (C_{dl}). The double layer capacitance (C_{dl}) is harmonious towards electrochemical active surface area (ECSA) as related by given equation:

$$ECSA = C_{dl}/C_s \quad (3)$$

Where, C_s is specific charge resistance of the working electrode. In alkaline electrolyte media, the regular C_s value of metal oxide was considered as 40 $\mu\text{F cm}^{-2}$ to determine electrochemical surface area (ECSA). The chronoamperometry (CA) study was performed on steady applied potential in both alkaline 1 M KOH and 1 M KOH + Seawater solution to investigate durability of the resulting catalyst.

To evaluate the real ability of the developed electrocatalyst, especially in seawater, the faradaic efficiency of CCV-2 has been determined using completely sealed H-cell system with a gas separator membrane in between using alkaline real seawater (1 M KOH + Seawater) as electrolyte. The chronoamperometric (CA) study of CCV-2 catalyst was

analysed in three electrode system applying 1.69 V vs RHE for 4 min and reaching a current of 0.074 A. Experimentally the evolved O₂ was determined using an oxygen sensor and theoretically the number of moles of oxygen (O₂) produced at anode can be determined from Faraday's second law as given below:

$$n_{theoretical}(O_2) = \frac{Q}{nF} = \frac{I \times t}{nF} \quad (4)$$

Where, i (A) is the reaching current at applied potential, t (sec) is the duration, n (4) is the number of electrons involved during OER and F (96485 s A mol⁻¹) is Faraday constant. Finally, the faradaic efficiency (FE) of the catalyst can be determined as following equation:

$$\text{Faradaic efficiency (FE)} = \frac{n_{O_2}(\text{experimental})}{n_{O_2}(\text{theoretical})} \times 100 = 92.39\% \quad (5)$$

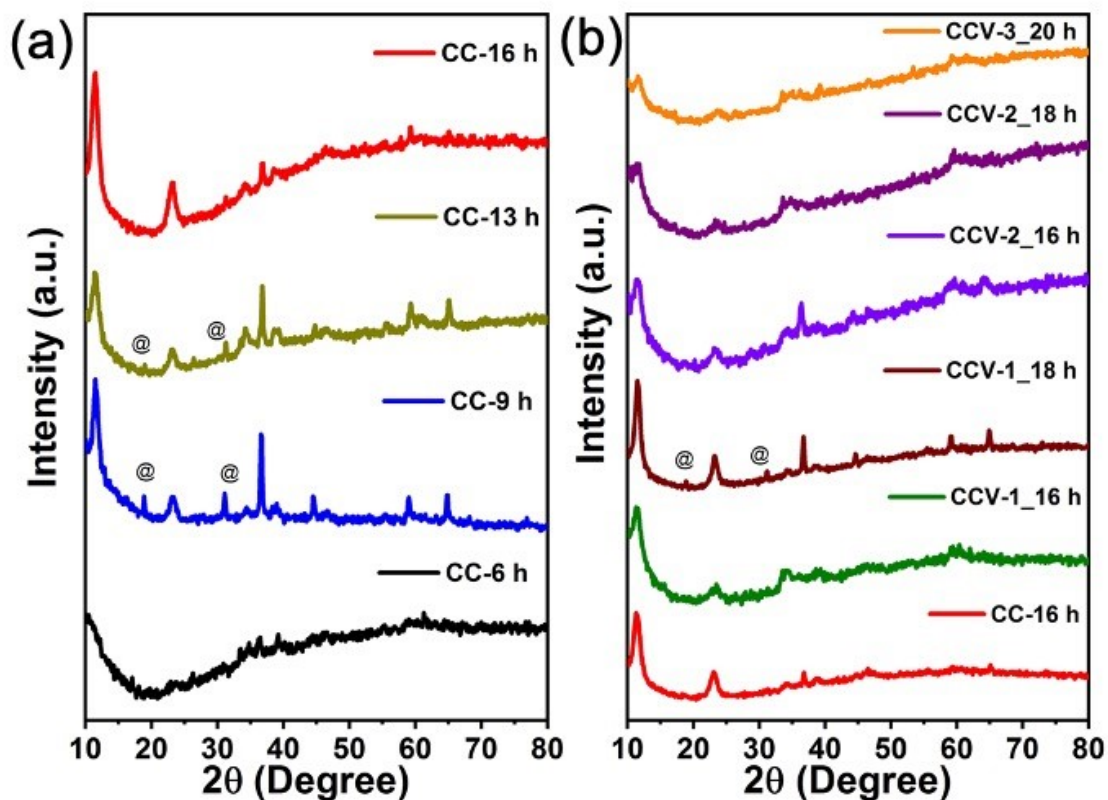


Figure S1: (a) XRD pattern of CoCr LDH at different durations (6h, 9h, 13h, and 16h) at 120 °C. (b) XRD pattern of CoCrV LDH with different V content at different durations (16h, 18h and 20h) maintaining 120 °C temperature. While CCV-1 requires 16h of reaction duration like CC, CCV-2 and CCV-3 require reaction durations of 18h and 20h, respectively to achieve LTH structure without presence of any metal hydroxides.

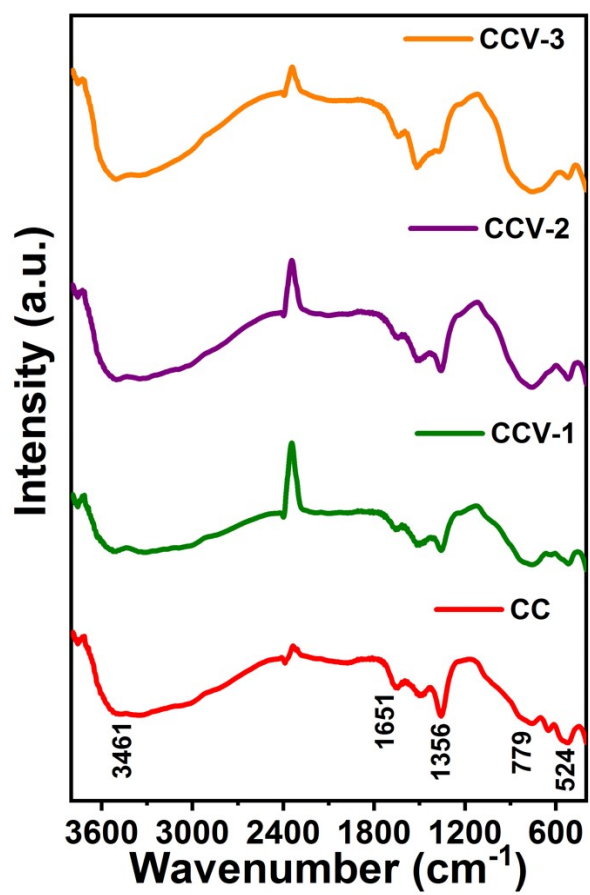


Figure S2: FTIR spectra of CC LDH and CCV LTHs materials.

Table S1: Reaction parameters and precursor concentrations used for developed CoCr LDH and CoCrV LTHs.

Samples	Reaction temperature/ duration	Co (mM)	Cr (mM)	V (mM)	V mol%	Total precursor conc.
CC	120 °C/16 h	2.0	1.0	0.0	0%	
CCV-1	120 °C/16 h	2.0	0.8	0.2	6.66%	3.0
CCV-2	120 °C/18 h	2.0	0.7	0.35	11.66%	
CCV-3	120 °C/20 h	2.0	0.5	0.5	16.66%	

Table S2: Elemental analysis of all samples using energy dispersive spectrum (EDX) showing atomic% of elements.

Samples	Co (atomic %)	Cr (atomic %)	V (atomic %)
CC	18.42	9.81	0
CCV-1	23.48	8.33	1.87
CCV-2	21.4	6.2	3.5
CCV-3	18.6	4.7	4.1

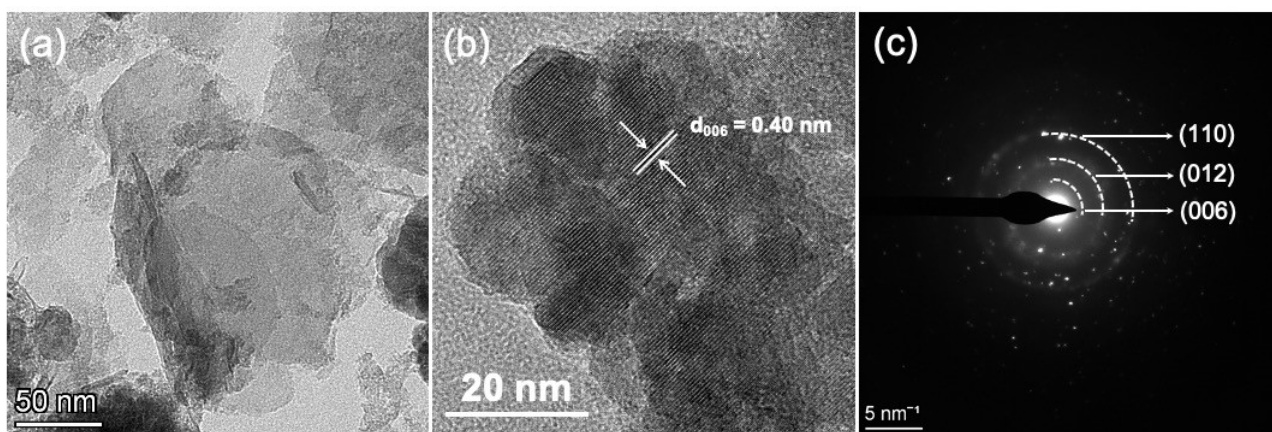


Figure S3: (a) TEM, (b) HR-TEM and (c) corresponding SAED pattern of CoCr LDH.

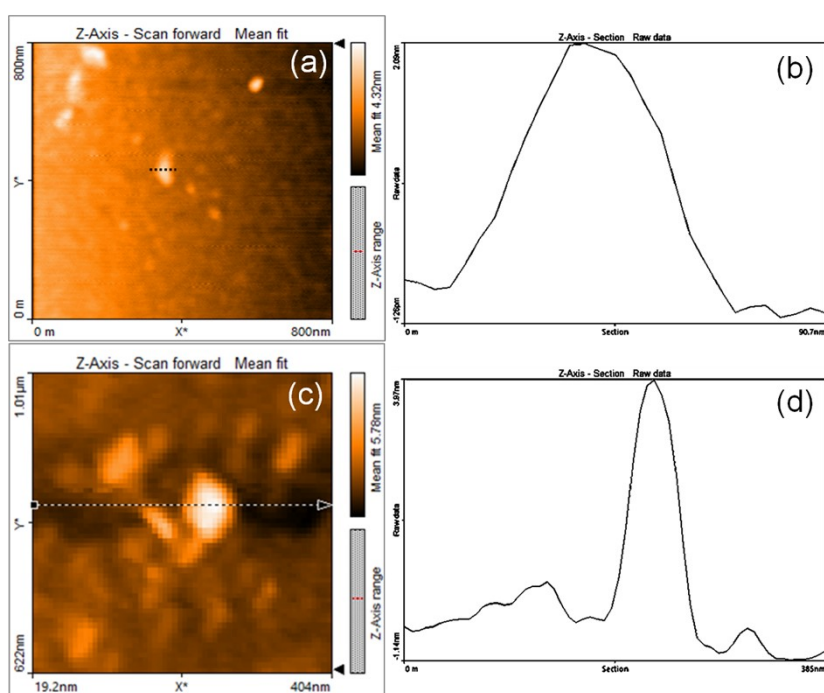


Figure S4: AFM image and corresponding height profile of (a-b) CC and (c-d) CCV-2.

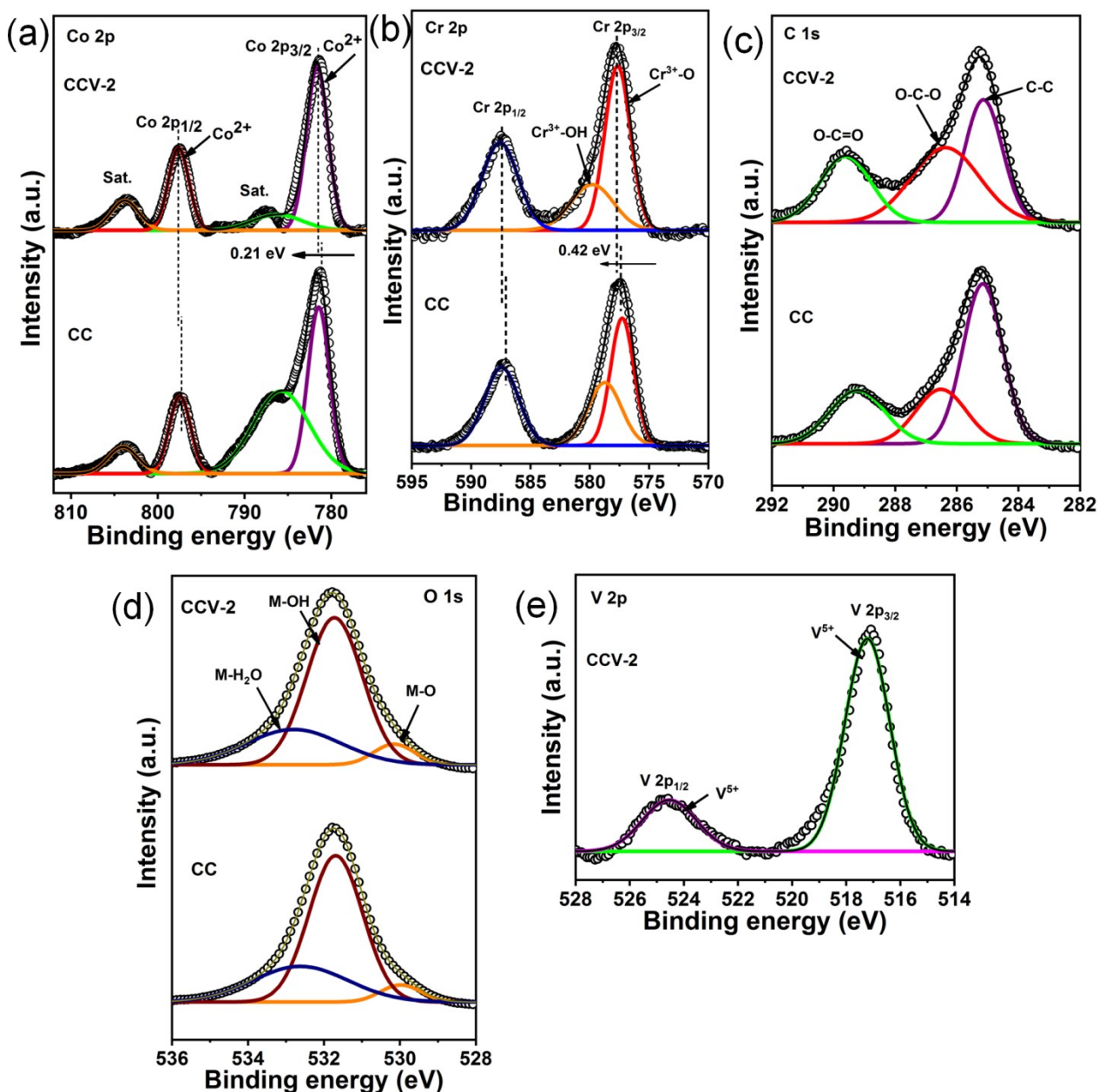


Figure S5. High resolution XPS spectra of (a) Co $2p$, (b) Cr $2p$, (c) C $1s$, (d) O $1s$ and (e) V $2p$ for CC and CCV-2.

The high resolution Co $2p$ spectra of both CC and CCV-2 show the presence of two major peaks for Co $2p_{1/2}$ and Co $2p_{3/2}$ along with their corresponding shake-up satellite peaks indicating the presence of Co(II). A slight positive shift (0.21 eV) of the Co $2p_{3/2}$ and Co $2p_{1/2}$ peaks towards higher binding energy can be noticed after insertion of V into the pristine CC, indicating possible electronic communication in-between Co and V in CCV-2. The Cr $2p$ spectra consists of two broad peaks for Cr $2p_{3/2}$ and Cr $2p_{1/2}$ for both CC and CCV-2. Furthermore, the Cr $2p_{3/2}$ spectrum can be deconvoluted into two peaks at 577.26 eV and 578.73 eV corresponding to Cr⁺³-O and Cr⁺³-OH

states, respectively, for CC, which also shows a positive shift (0.42 eV) in CCV-2 at 577.68 eV ($\text{Cr}^{+3}-\text{O}$) and 579.2 eV ($\text{Cr}^{+3}-\text{OH}$). This indicates a strong electronic inter-action of Cr with V in CCV-2. The high resolution V $2p$ spectrum of CCV-2 is composed of two peaks at 517.21 eV and 524.53 eV, corresponding to V $2p_{3/2}$ and V $2p_{1/2}$, respectively, for the V^{+5} oxidation state as shown in Fig. S5(e). The high resolution C 1s spectra of both CC and CCV-2 can be deconvoluted into three major peaks with a broad peak located at 289.23 eV assigned to $\text{O}-\text{C}=\text{O}$, confirming the presence of CO_3^{2-} with a noticeable increase in the peak intensity in CCV-2 compared to that in CC indicating a higher number of carbonate molecules in the inter-layer spacing in line with the FTIR results (Fig. S5(c)). In both CC and CCV-2, the O 1s spectrum can be deconvoluted into three peaks located at the binding energies of 530.1 eV, 531.7 eV and 532.7 eV, which are primarily believed to be from the contributions of metal-oxide ($\text{M}-\text{O}$), surface hydroxyl ($\text{M}-\text{OH}$) and absorbed H_2O , respectively.

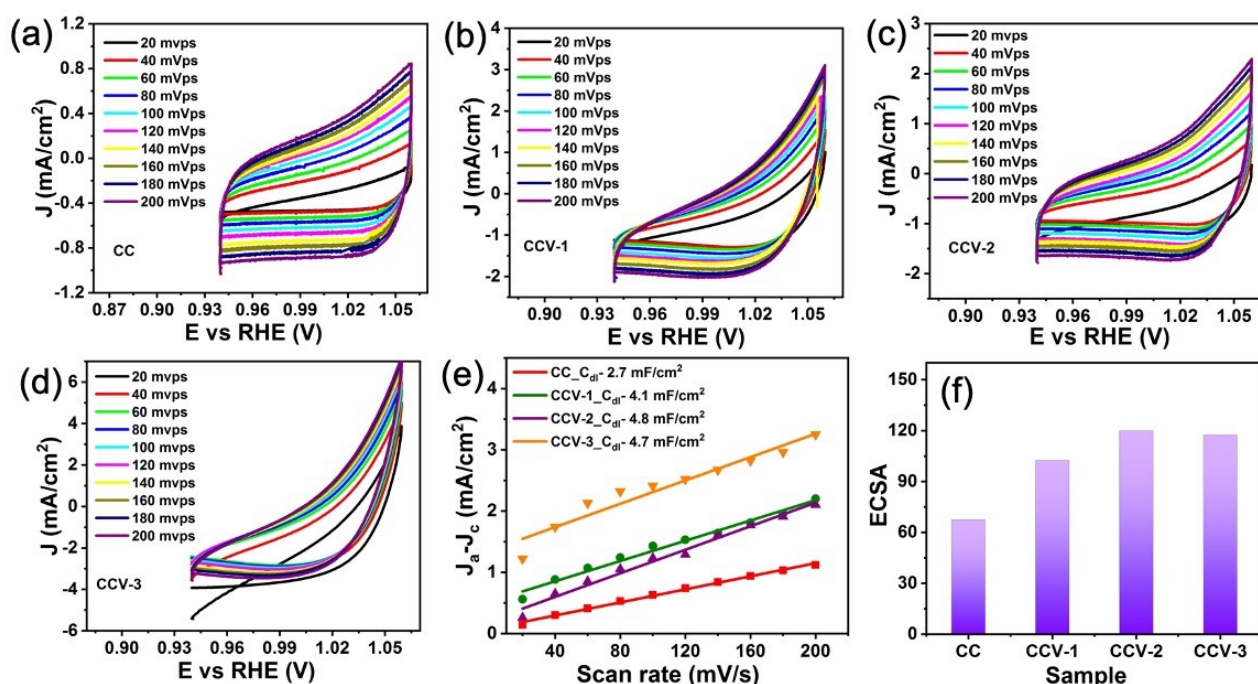


Figure S6: Cyclic Voltammograms (CV) obtained in non-Faradaic region at various scan rates for (a) CC, (b) CCV-1, (c) CCV-2 and (d) CCV-3 LTHs. (e) Plot of current density difference ($J_a - J_c$) versus scan rates to obtain double layer capacitance (C_{dl}) of CC LDH and CCV LTHs. (f) Electrochemical active surface area (ECSA) of CC LDH and all combinations CCV LTHs.

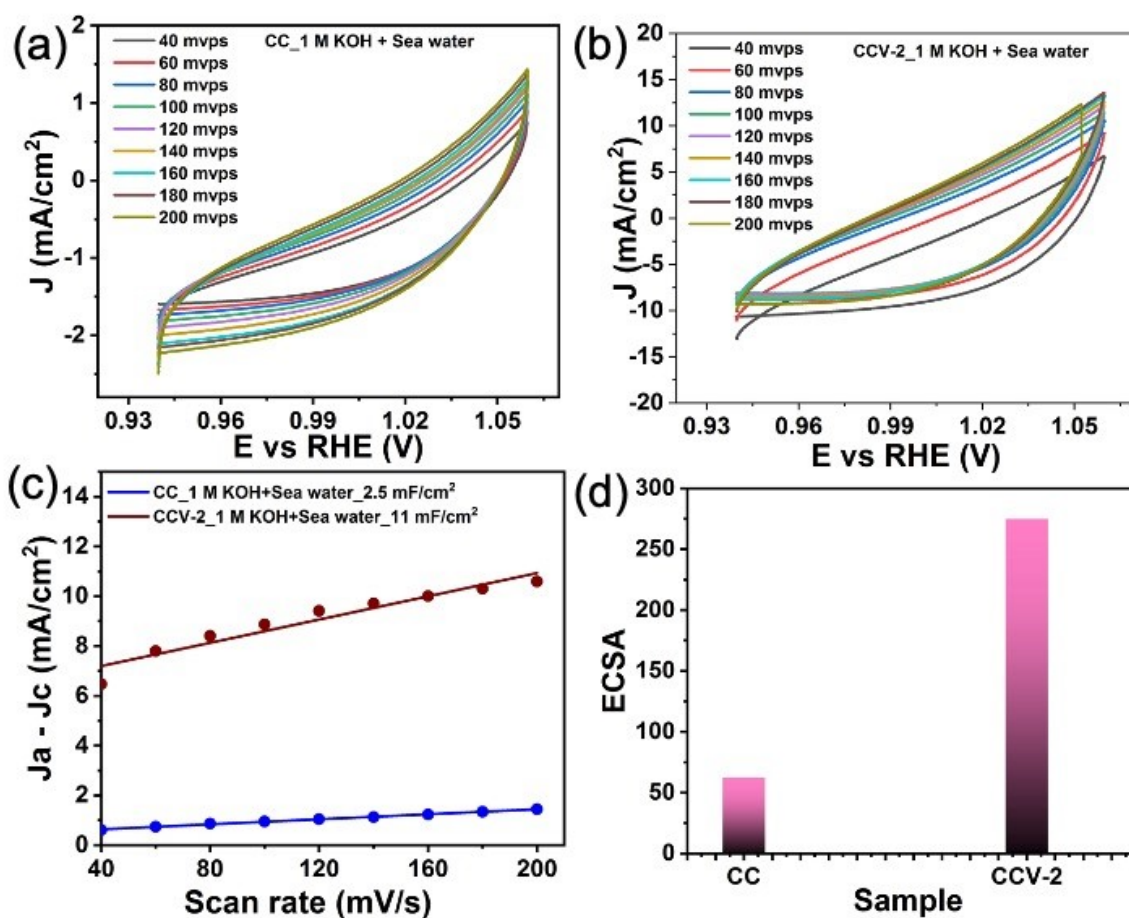


Figure S7. Cyclic Voltammograms (CV) obtained in non-Faradaic region at various scan rates for (a) CC LDH and (b) CCV-2 LTH in 1 M KOH + Seawater electrolyte. (c) Plot of current density difference ($J_a - J_c$) versus scan rates to obtain double layer capacitance (C_{dl}) of CC LDH and CCV-2 LTH. (d) Electrochemical active surface area (ECSA) of CC LDH and CCV-2 LTH in 1 M KOH + Seawater electrolyte media.

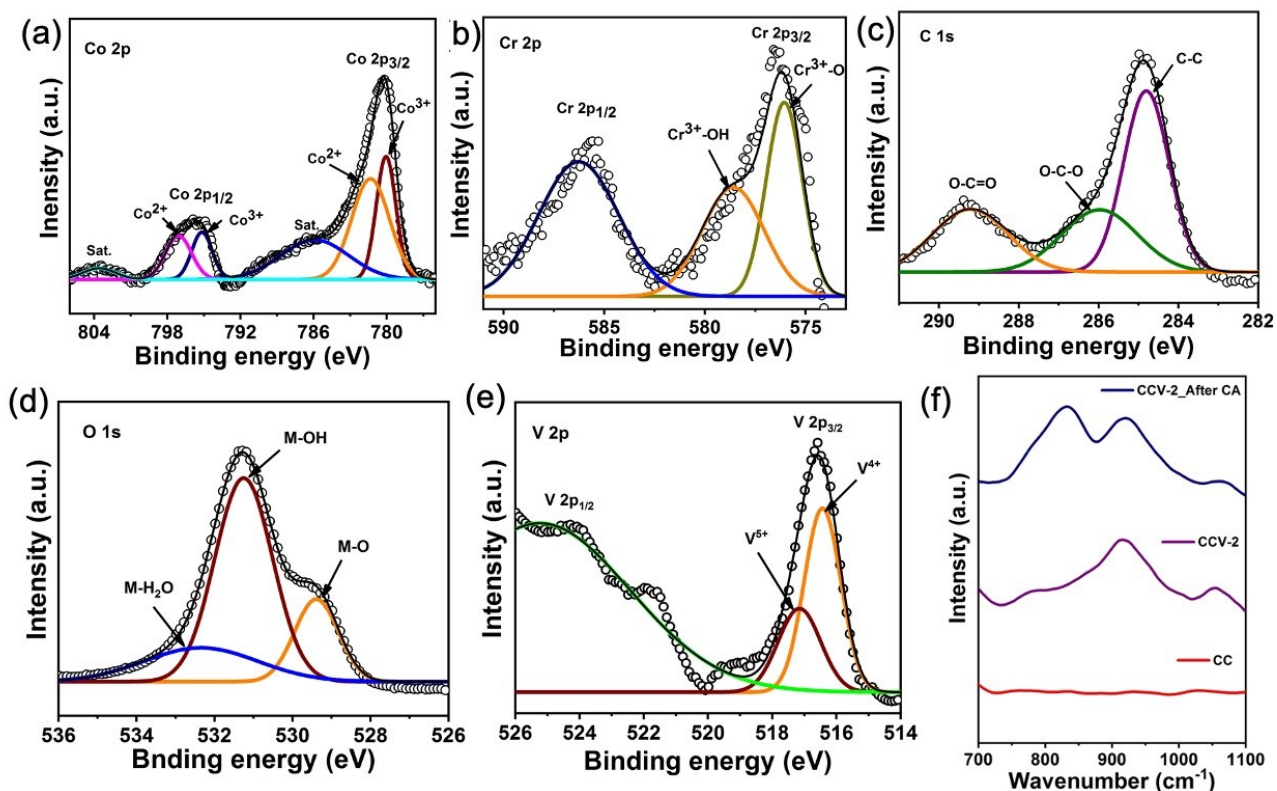


Figure S8. High resolution XPS spectra of (a) Co 2p, (b) Cr 2p, (c) C 1s, (d) O 1s and (e) V 2p for CCV-2 after chronoamperometry (CA) test in alkaline real seawater electrolyte solution. (f) Raman spectrum of CC LDH, before and after chronoamperometry (CA) test of CCV-2 LTH in alkaline seawater.

Focusing on the stretching mode of vanadyl oxygen bond in Raman spectra, while CC sample indicates flat spectra for obvious reason within the medium range of 700 – 1100 cm^{-1} , CCV-2 sample before the stability test shows two broad peaks at 920 cm^{-1} and 1050 cm^{-1} , assigned for $\text{V}^{5+}\text{-O}$. Very interestingly, after long exposure in real seawater electrolyte during chronoamperometry study an appearance of an additional peak towards lower frequency at 840 cm^{-1} is observed, which is believed to be due to $\text{V}^{4+}\text{-O}$, as also reported elsewhere^{S1-S3}.

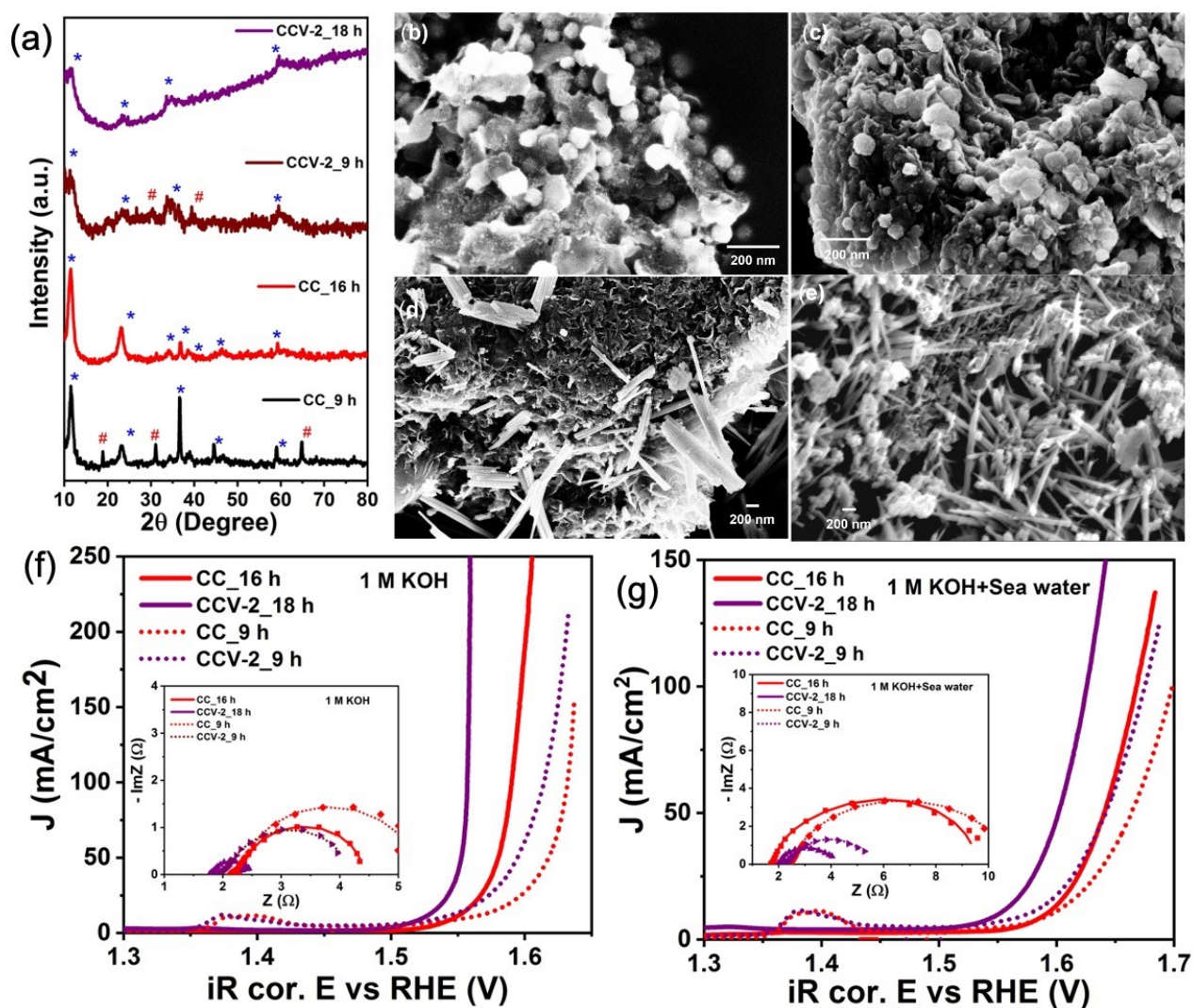


Figure S9. (a) X-ray diffraction pattern of CC and CCV-2 samples obtained at different reaction durations (* indicates characteristic LDH peaks and # indicates characteristic hydroxide peaks). (b-e) FESEM image of CC and CCV-2 samples obtained at 9h (b), 16h (c) for CC and 9h (d), 18h (e) for CCV-2. (f, g) LSV plots of CC and CCV-2 samples obtained in different reaction durations in 1 M KOH (f) and 1 M KOH + Seawater (g) electrolytes (*inset*: corresponding EIS plots).

It was observed that at shorter reaction duration of 9h in both the cases of CC and CCV, the formation of hydroxides cannot be avoided and the development of LDH or LTH structures require longer and optimized reaction duration as indicated in the XRD pattern

shown in Figure S9(a). The morphology of the samples remain almost identical regardless to reaction durations (Figure S9(b-e)). Very importantly, it has been found that electrocatalytic activity of the prepared materials in 1M KOH depends much on the development of LDH or LTH structures. In any case, the developed CCV-2 LTH without any trace of hydroxides obtained after 18 h of hydrothermal reaction showed best electrocatalytic activity compared to the sample obtained at 9h of reaction duration with mixed LTH and hydroxide structure. Similarly, CC LDH obtained after 16h of reaction duration without any presence of hydroxides showed better performance compared to shorter duration counterpart (9h) containing hydroxide traces. The similar observations have also been found in alkaline real seawater electrolyte, which confirms the fact that LDH or LTH structures are important to exhibit best possible electrocatalytic activity.

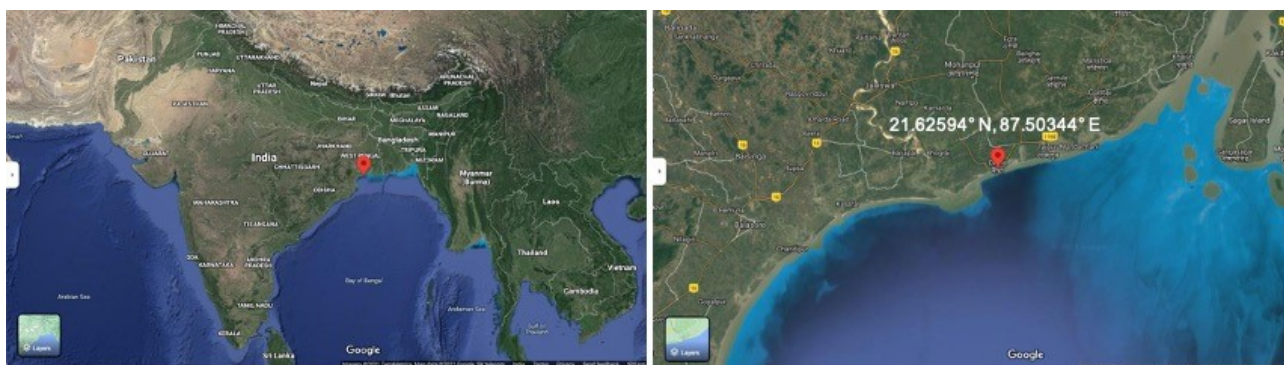


Figure S10: The seawater collection location shown in satellite view taken from Google Map.

Table S3: Comparison table of electrocatalytic OER activities of various LDHs as electrocatalyst in 1 M KOH alkaline electrolyte media.

Materials	η (mV) @ 10 mA/cm ²	η (mV) @ 100 mA/cm ²	Tafel slope (mV/dec)	Durability (h)	Reference
Ni _{0.75} V _{0.25} -LDH	300	350 @ 44 mA/cm ²	50	25	S4
NiFe-LDH	300	--	40	13	S5
NiFeCr-LDH	280	--	130	6	S6
V _{0.3} -CoFe-LDH	240	--	74	24	S7
NiFeV-LDH	195 @ 20 mA/cm ²	233	42	18	S8
CoCr-LDH	400 @ 20 mA/cm ²	--	81	12	S9
NiCr-LDH	--	319	22.9	30	S10
NiCu _x -LDH	290	355	45	50	S11
NiFeMn-LDH	289 @ 20 mA/cm ²	--	47	16	S12
FeNiCo-LDH	230	--	42	--	S13
NiFe-LDH	230	--	47	100	S14
NiCoFe ALDHs/CFC	239	--	32	12	S15
CoFe LDH/NF	300	420	83	10	S16
NiCoCHH (1-1)	238	--	190	12	S17
Co ₈ Fe ₁ -LDH	262	306	42	20	S18
CoFe-LDH@gC ₃ N ₄	275	--	58	12	S19
CoFe LDH/MWCNT/rGO	330	--	77.73	12	S20
CoMn LDH	324	--	43	14	S21
CoCrV LTH	291	320	39	100	This work

Table S4: Comparison table of electrocatalytic OER activities of various catalysts in real and as well as stimulated seawater.

Materials	Electrolyte	η (mV) @ 10 mA/cm ²	η (mV) @ 100 mA/cm ²	Durability (h)	Reference
Se_NiFe LDH	1 M KOH + 1 M NaCl	220 @ 20 mA/cm ²	--	100	S22
Ni ₃ FeN@C/NF	1 M KOH + 0.5 M NaCl	--	283	--	S23
CoFe LDH/Ti	Stimulated Sea water	530	--	8	S24
Na ₂ Co _{1-x} Fe _x P ₂ O ₇ /C@CC	0.1 M KOH + 0.5 M NaCl	285	1.6 V	100	S25
Na ₂ Co _{1-x} Fe _x P ₂ O ₇ /C@CC	1 M KOH + Sea water	325	--	50	S25
NiMoN@NiFeN	1 M KOH + 0.5 M NaCl	--	286	--	S26
NiMoN@NiFeN	1M KOH+ Sea water	--	307	--	S26
NiFeB _x @NiFe alloy (MOEE)	30 wt% KOH + 0.5 M NaCl	--	328	100	S27
FTO/NiO	1 M KOH + 0.5 M NaCl	401	--	8	S28
Co ₃ O ₄ -MnO ₂	0.5 M KOH + 0.5 M NaCl	450	--	--	S29
Co ₃ O ₄ -MnO ₂	Mediterranean Seawater	500	--	--	S29
Co-Fe-O-B-10	1 M KOH + 0.5 M NaCl	294	434	20	S30
NiFe LDH	0.1 M KOH + 0.5 M NaCl	359	--	2	S31
NiFe LDH S350	1 M KOH + 0.5 M NaCl	--	296	12	S32
Fe ₂ O ₃ /NiO	1 M KOH + 1 M NaCl	--	252 @ 1000 mA/cm ²	50	S33
Fe ₂ O ₃ /NiO	1 M KOH + Sea water	--	291 @ 1000 mA/cm ²	50	S33
Fe-Co-S/Cu ₂ O/Cu	1 M KOH + 0.5 M NaCl	--	390	30	S34
Ni/NiFe LDH	1 M KOH + 0.5 M NaCl	240	313	--	S35
Ni/NiFe LDH	1 M KOH + Sea water	247	303	100	S35
Ni ₂ P-Fe ₂ P/NF	1 M KOH+ Sea water	--	305	36	S36
CoCrV LTH	1 M KOH + 1 M NaCl	300	365	--	This work
	1 M KOH + Sea water	320	395	24	

References

- [S1] S. H. Lee, H. M. Cheong, M. Je. Seong, P. Liu, C. E. Tracy, A. Mascarenhas, J. R. Pitts, S. K. Deb, *Journal of Applied Physics*, **2002**, 92, 1893-1897.
- [S2] P. Shvets, O. Dikaya, K. Maksimova, A. Goikhman, *Journal of Raman Spectroscopy*, **2019**, 50, 8, 1226-1244.
- [S3] F. U. Begara, A. Crunteanu, J. P. Raskin, *Applied Surface Science*, **2017**, 403, 717-727.
- [S4] K. Fan, H. Chen, Y. Ji, H. Huang, P. M. Claesson, Q. Daniel, B. Philippe, H. Rensmo, F. Li, Y. Luo, L. Sun, *Nat. Commun.*, **2016**, 7, 11981.
- [S5] F. Song, X. Hu, *Nat. Commun.*, **2014**, 5, 4477.
- [S6] Y. Yang, L. Dang, M. J. Shearer, H. Sheng, W. Li, J. Chen, P. Xiao, Y. Zhang, R. J. Hamers, S. Jin, *Adv. Energy Mater.*, **2018**, 8, 170318.
- [S7] B. Singh, A. Indra, *Dalton Trans.*, **2021**, 50, 2359-2363.
- [S8] P. Li, X. Duan, Y. Kuang, Y. Li, G. Zhang, W. Liu, X. Sun, *Adv. Energy Mater.*, **2018**, 8, 1703341.
- [S9] C. Dong, X. Yuan, X. Wang, X. Liu, W. Dong, R. Wang, Y. Duan, F. Huang, *J. Mater. Chem. A*, **2016**, 4, 11292-11298.
- [S10] W. Ye, X. Fang, X. Chen, D. Yan, *Nanoscale*, **2018**, 10, 19484-19491.
- [S11] Y. S. Xie, Z. Wang, M. Ju, X. Long, S. Yang, *Chem. Sci.*, **2019**, 10, 8354-8359.
- [S12] Z. Lu, L. Qian, Y. Tian, Y. Li, X. Sun, X. Duan, *Chem. Commun.*, **2016**, 52, 908–911.
- [S13] X. Long, S. Xiao, Z. Wang, X. Zheng, S. Yang, *Chem. Commun.*, **2015**, 11, 1120-1123.
- [S14] X. Zhang, Y. Zhao, Y. Zhao, R. Shi, G. I. N. Waterhouse, *Adv. Energy Mater.*, **2019**,

9, 1900881.

[S15] A. L. Wang, H. Xu, G. R. Li, *ACS Energy Lett.*, **2016**, 1, 2, 445-453.

[S16] L. Feng, A. Li, Y. Li, J. Liu, L. Wang, L. Huang, Y. Wang, X. Ge, *ChemPlusChem*, **2017**, 82, 483-488.

[S17] K. Karthick, S. Subhashini, R. Kumar, S. S. Markandaraj, M. M. Teepikha, S. Kumdu, *Inorg. Chem.*, **2020**, 59, 22, 16690-16702.

[S18] J. Zhao, X. R. Wang, F. W. Chen, C. He, X. J. Wang, Y. P. Li, R. H. Liu, X. M. Chen, Y. J. Hao, M. Yang, F. T. Li, *Inorg. Chem. Front.*, **2020**, 7, 737-745.

[S19] M. Arif, G. Yasin, M. Shakeel, M. A. Mushtaq, W. Ye, X. Fang, S. Ji, D. Yan, *Mater. Chem. Front.*, **2019**, 3, 520-531.

[S20] Y. J. Yang, M. Duan, C. Yan, D. Zhao, C. Jiang, X. Duan, X. Song, *J. Electroanal. Chem.*, **2020**, 856, 113697.

[S21] F. Song, X. Hu, *J. Am. Chem. Soc.*, **2014**, 136, 47, 16481-4.

[S22] W. H. Hung, B. Y. Xue, T. M. Lin, S. Y. Lu, I. Y. Tsao, *Mater. Today Energy*, **2019**, 19, 100575.

[S23] B. Wang, M. Lu, D. Chen, Q. Zhang, W. Wang, Y. Kang, Z. Fang, G. Pang, S. Feng, *J. Mater. Chem. A*, **2021**, 9, 13562-13569.

[S24] F. Cheng, X. Feng, X. Chen, W. Lin, J. Rong, W. Yang, *Electrochim. Acta*, **2017**, 251, 336-343.

[S25] H. J. Song, H. Yoon, B. Ju, D. Y. Lee, D. W. Kim, *ACS Catal.*, **2020**, 10, 1, 702-709.

[S26] L. Yu, Q. Zhu, S. Song, B. McElhenny, D. Wang, C. Wu, Z. Qin, J. Bao, Y. Yu, S. Chen, Z. Ren, *Nat. Commun.*, **2019**, 10, 5106.

[S27] J. Li, Y. Liu, H. Chen, Z. Zhang, X. Zou, *Adv. Funct. Mater.*, **2021**, 31, 2101820.

[S28] J. Juodkazyte, B. Sebek, I. Seveckaja, M. Petruleviciene, S. Butkute, V. Jasulaitiene, A. Selskis, R. Ramanauskas, *Int. J. Hyd. Energy*, **2019**, 44, 5929-5939.

[S29] L. Bigiani, D. Barreca, A. Gasparotto, T. Andreu, J. Verbeeck, C. Sada, E. Modin, O. Lebedev, J. R Morante, C. Maccato, *Appl. Catal. B: Environmental*, **2021**, 284, 119684.

- [S30] S. Gupta, M. Forster, A. Yadav, A. J. Cowan, N. Patel, M. Patel, *ACS Appl. Energy Mater.*, **2020**, 3, 8, 7619-76-28.
- [S31] F. Dionigi, T. Reier, Z. Pawolek, M. Glied, P. Strasser, *ChemSusChem*, **2016**, 9, 962-972.
- [S32] S. Y. Jung, S. Kang, K. M. Kim, S. Mhin, J. C. Kim, S. J. Kim, E. Enkhtuvshin, S. Choi, H. Han, *Appl. Surf. Sci.*, **2021**, 568, 150965.
- [S33] L. Li, G. Zhang, B. Wang, D. Zhu, D. Liu, Y. Liu, S. Yang, *ACS Appl. Mater. Interfaces*, **2021**, 13, 31, 37152-37161.
- [S34] J. Sun, P. Song, H. Zhou, L. Lang, X. Shen, Y. Liu, X. Cheng, X. Fu, G. Zhu, *Appl. Surf. Sci.*, **2021**, 567, 150757.
- [S35] M. Ning, L. Wu, F. Zhang, D. Wang, S. Song, T. Tong, J. Bao, S. Chen, L. Lu, Z. Ren, *Mater. Today Physics*, **2021**, 19, 100419.
- [S36] L. Wu, L. Yu, F. Zhang, B. McElhenny, D. Luo, A. Karim, S. Chen, Z. Ren, *Adv. Funct. Mater.*, **2021**, 31, 2006484.